applied sciences

MDPI

Article

Controlled Release Using Gas Detonation in Needle-Free Liquid Jet Injections for Drug Delivery

Rocco Portaro [1], Jad Sadek [1], Han Xu [2] and Hoi Dick Ng [1,*]

[1] Department of Mechanical, Industrial and Aerospace Engineering, Concordia University, Montreal, QC H3G 1M8, Canada
[2] National Key Laboratory of Transient Physics, Nanjing University of Science and Technology, Nanjing 210094, Jiangsu, China
* Correspondence: hoing@encs.concordia.ca; Tel.: +1-514-848-2424 (ext. 3177)

Received: 6 May 2019; Accepted: 29 June 2019; Published: 4 July 2019

Abstract: The advent of new drug therapies has resulted in a need for drug delivery that can deal with increased drug concentration and viscosities. Needle-free liquid jet injection has shown great potential as a platform for administering some of these revolutionary therapies. This investigation explores the detonative combustion phenomenon in gases as a simple and efficient means of powering needle-free liquid jet injection systems. A preliminary, large-scale prototype injector was designed and developed. In contrast with the widely used air-powered and electrical driven needle-free injectors, the proposed detonation-driven mechanism provides equivalent liquid jet evolution and performance but can efficiently provide a controllable power source an order magnitude higher in strength by varying combustible mixtures and initial conditions. The simplicity and power output associated with this concept aid in improving current needle-free liquid injector design, especially for delivery of high volume, high viscosity drugs, including monoclonal antibodies, which target precise locations in skin tissue.

Keywords: needle-free technology; liquid jet injection; detonative combustion; drug delivery; controlled release

1. Introduction

Drug delivery without the use of hypodermic needles has been a long-term objective within the medical field [1]. Among different needle-free technology, liquid jet injectors can deliver medication to a target area by rupturing the skin through the pressure exerted by a liquid jet. The basic mechanism involves the use of a power source to compress a liquid and expel it through an orifice [2]. This technology has been in existence since the early 20th century, and during that period the effectiveness in eliminating bio-hazardous waste and delivering a broad range of medication have made this technology ideal for mass immunization [3]. However, drawbacks such as pain, bruising, splash back, hematomas, excessive penetration and cross contamination have limited the use of needleless jet injection for both mass immunization as well as individual use [4–6].

Recently, the technology has gained renewed interest for delivering both micro- and macromolecules and advancements in fluid dynamic research have aided in propelling this technology as an ideal platform for newly developed drug therapies, including monoclonal antibodies [7,8]. Notably, jet injectors are capable of targeting shallow layers of the skin such as the epidermis as well as sensitive organs [9]. Furthermore, liquid jet injectors can also be used for targeting diseases which benefit from localized treatment techniques.

Parametric studies and technological advancements throughout the years have enhanced the performance and controllability of needleless injectors. A better understanding of the driving force

and the fluid mechanics have also led to better optimization of the device in terms of delivery depth and controllability of drug flow, resulting in better drug distribution. The majority of engineering studies analyze spring- or gas-powered injectors, e.g., [10–19], whilst experimental prototypes utilize electrically driven power sources in order to provide real-time control of jet pressure, e.g., [20–22]. Highly experimental techniques also include electrical current discharge and laser-based systems, to generate highly focused, pulsed liquid microjets from vapor bubble collapse [23–26].

However, new emerging trends in needle-free technology are creating a need for delivering higher volume as well as highly viscous injections [3]. The needle-free injector's precision as well as its ability to target deep areas of tissue such as muscle, provide good building blocks for use with new drug therapies. Nevertheless, there is a need for power sources that are sufficiently strong, and which can be accurately controlled in order to provide a liquid jet with velocities on the order of 100–200 m/s, predictable penetration depth, large-volume delivery efficiency, as well as cope with an increase in drug viscosities observed with new drug formulations used for emerging medical treatments [27,28].

Apart from drug delivery in humans, needle-free liquid jet injection technology also attracts significant interest for animal vaccination [29–32]. It provides an efficient mean to achieve continuous injection for mass vaccination of farmed livestock. It is worth noting that different livestock such as cattle or swine have rather different skin properties and often require different vaccine doses, therefore, flexible power must be provided to the needle-free injection system.

This study explores the use of combustion to generate the required power in order to drive the needle-free injector. Specifically, the detonative combustion mode is considered in this work. It makes use of the pressure increase across the detonation wave in order to drive the injection piston and pressurize the medication. The present study serves to highlight the feasibility of using gaseous detonation-driven power sources as a convenient and efficient means of powering liquid jet injections.

2. Fundamentals and Methods

A detonation is a supersonic, combustion-driven compression wave across which there is a significant pressure increase. It has been suggested that by properly harnessing the potential of the detonative combustion, the energy release from such a process can be used for power generation and propulsion applications [33,34]. The previous works by Golub et al. [35] and Krivokoritov et al. [36] have demonstrated the potential of using detonation waves in stoichiometric hydrogen-air mixtures at atmospheric conditions for needle-free injections and delivering 0.2 mL of liquid water at a drop speed on the order of 70 m/s by means of a deformable diaphragm. In this study, a conventional piston-driven jet generation mechanism is employed. The reason is two-fold: to design a device capable for large volume drug delivery and to compare other types of injector systems (e.g., gas-powered or Lorentz-force actuated) which use the same impact mechanism. A more sensitive combustible mixture, namely, pre-mixed stoichiometric acetylene-oxygen mixture at sub-atmospheric initial pressure in the range of 25 to 60 kPa is used to provide safe operating conditions. The combustible is prepared using the method of partial pressures in a separate mixing tank.

A schematic of the experimental detonation-driven liquid jet injection prototype is shown in Figure 1. The setup combines a detonation tube made of a 590-mm long, circular, steel tube with an inner diameter D = 26.4 mm with a custom-made needle-free liquid jet injector module. The injector module is made of a moving plunger and a metering screw used to adjust the drug delivery volume. An orifice micronozzle (O'Keefe Controls Co.) is threaded at the end of the injector for the jet generation. Table 1 illustrates the important physical characteristics of the injector module.

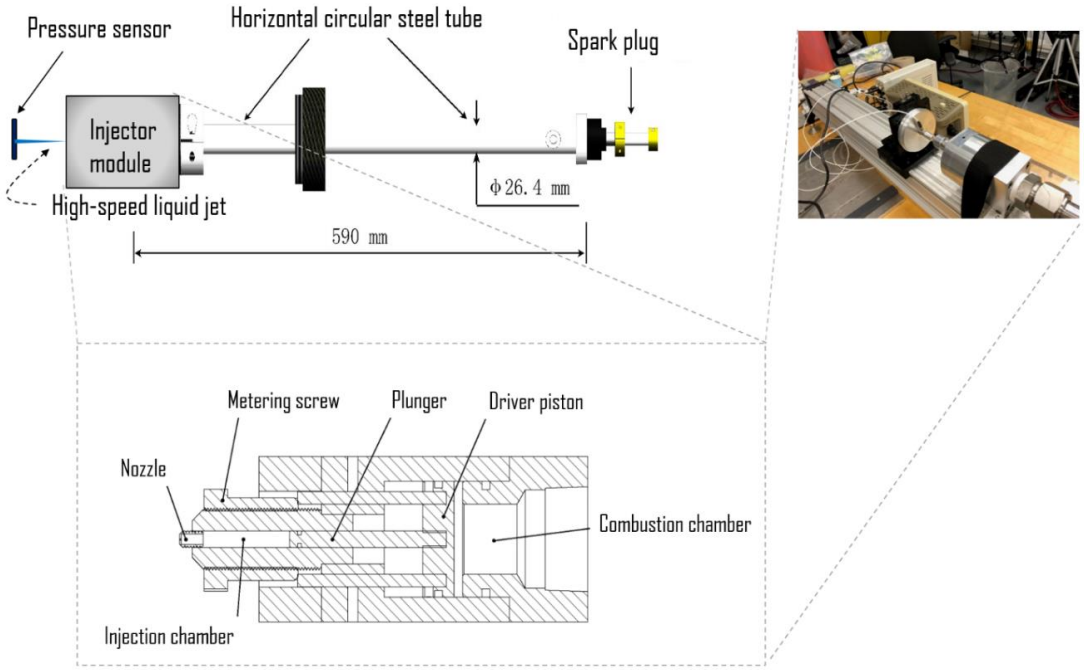

Figure 1. Schematic of the experimental setup consisted of the detonation tube and the needle-free liquid jet injector module.

Table 1. Injector module parameters.

Injector Parameters	
Orifice nozzle diameter, D_o	200 μm
Driver diameter, D_d	44.4 mm
Piston diameter, D_p	6.35 mm
Mass of the piston, M_p	150 g
Liquid column, L	20 mm

The injector is filled with water as its working fluid, density $\rho_o = 1000$ kg/m^3 and fluid bulk modulus $B = 2.18 \times 10^9$ N/m^2. In this investigation, the delivery volume is set at 0.6 mL. A Chapman–Jouguet (CJ) detonation is initiated at the closed end of the tube via a high-voltage capacitor spark discharge and propagates along the tube until it impacts the injector's piston, which in turn generates the high-speed liquid jet through the orifice nozzle. A PCB Model 209C11 miniature force sensor is used for the jet pressure measurement. This is accomplished using the orifice nozzle diameter, i.e., by dividing the force sensor reading of the jet impact stagnation surface by the exit orifice area. The force sensor is clamped perpendicular to the injector's nozzle exit. The output of the transducer is amplified and gathered using a RIGOL DS1102E oscilloscope with 1G sample/second.

A sketch of the detonation reflection gas dynamic process is shown in Figure 2. Properties across a detonation wave can be computed thermodynamically using an equilibrium control volume analysis. By solving the one-dimensional conservation equations together with the tangency requirement between the Rayleigh line and the equilibrium Hugoniot curve, (i.e., Chapman–Jouguet criterion), the detonation velocity D_{CJ} and its thermodynamic equilibrium states can be computed. Chemical equilibrium software such as the NASA Computer program, Chemical Equilibrium with Applications (CEA) [37], provide such calculations. For the stoichiometric acetylene-oxygen mixture at different initial pressures, the CJ detonation pressure is plotted in Figure 3 (dotted line).

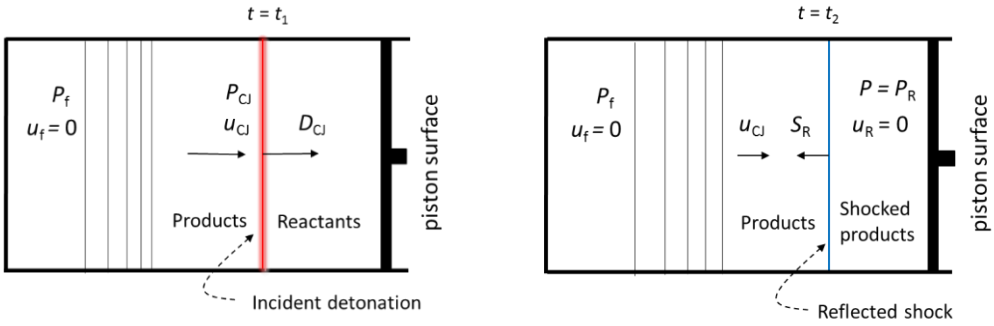

Figure 2. A sketch showing different gas dynamic states of the detonation reflection process.

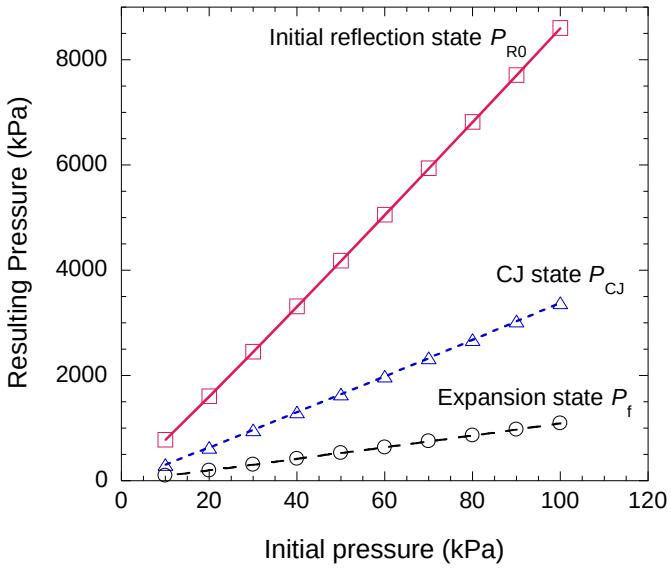

Figure 3. Incident Chapman–Jouguet (CJ) detonation pressure, reflected pressure and expansion pressure for stoichiometric C_2H_2/O_2 mixture at various initial pressures.

The detonation propagates at D_{CJ} into the unburned reactants and impinges upon the plunger of the injector module at $x = L$. The detonation wave reflection results in an even higher pressure on the injector's piston. The resulting maximum pressure occurring at the moment of reflection can be estimated using a simple gas dynamic analytical model based on the Rankine–Hugoniot equations for a constant-γ ideal gas [38,39], i.e.:

$$\frac{P_{R0}}{P_{CJ}} = \frac{5\gamma + 1 + \sqrt{17\gamma^2 + 2\gamma + 1}}{4\gamma} \tag{1}$$

where P_{CJ} is the CJ detonation pressure, P_{R0} the immediate reflected-detonation shock pressure, γ the ratio of specific heats. Taking an average $\gamma = 1.275$ at the detonation CJ state, $P_{R0} \approx 2.54\ P_{CJ}$. The CJ pressure and reflected pressure versus initial pressure of the combustible are plotted in Figure 3 shown by dotted and solid lines, respectively.

Due to the solid boundary at $x = 0$, a non-steady expansion wave—also referred to as the Taylor–Zel'dovich wave—follows behind the detonation lowering the pressure and temperature to match the boundary conditions. As shown in [40,41] and also recently in [42], the immediate reflected pressure P_{R0} will decay exponentially toward the final expansion pressure, i.e.,:

$$P_R(t) = \left(P_{R0} - P_f\right) exp\left[-\frac{t}{\tau}\right] + P_f \tag{2}$$

where τ is a time decay constant and $P_R(t)$ asymptotes to P_f within the typical injection period. P_f is the pressure behind the Taylor–Zel'dovich wave, which can be calculated using the isentropic relationship across the expansion:

$$P_f = P_{CJ}\left(\frac{c_f}{c_{CJ}}\right)^{2\gamma/(\gamma-1)} \tag{3}$$

where the sound speed c_f can be obtained by noting $u_f = 0$ at $x = 0$ end wall and using the Riemann invariants along the C^- characteristics for the detonation:

$$\Gamma_- = u_{CJ} - \frac{2c_{CJ}}{\gamma - 1} = -\frac{2c_f}{\gamma - 1} \tag{4}$$

where u_{CJ} is the flow velocity immediately behind the detonation. According to the Chapman–Jouguet criterion, u_{CJ} is equal to the detonation velocity D_{CJ} minus the sound speed at the CJ state, c_{CJ}. Hence:

$$c_f = \frac{\gamma + 1}{2}c_{CJ} - \frac{\gamma - 1}{2}D_{CJ} \tag{5}$$

The expansion pressure P_f is also plotted in Figure 3 given by the dashed line. The initial reflected shock pressure P_{R0} provides a sufficiently large driving force to punch the skin and generate the injection jet with high inertia and pressure after the expansion process P_f for the rate constant drug delivery.

To model the jet evolution and obtain its flow properties, a model was developed by Baker and Sanders [10] by performing a mass balance and force analysis on the injection device. Assuming that the water is incompressible, the jet pressure can be described by integrating the following expression:

$$\frac{dP_{jet}}{dt} = \frac{\left(B + P_{jet}\right)\frac{dx_p}{dt} - \frac{BA_o}{A_p}\sqrt{\frac{2P_{jet}}{\rho_o}}}{L - x_p} \tag{6}$$

where the piston acceleration driven by the detonation wave reflection is given by the following equation of motion derived from a force balance:

$$\frac{d^2x_p}{dt^2} = \frac{A_d P_R(t)}{M_p} - \frac{A_p P_{jet}(t)}{M_p} - \frac{F_{O-rings}(t)}{M_p\left|\frac{dx_p}{dt}\right|}\frac{dx_p}{dt} \tag{7}$$

It consists of the driving force generated by the reflected shock pressure (Equation (2)), the fluid pressurization, as well as frictional losses due to the O-ring sealing in the plunger, $F_{O\text{-}rings}(t)$. The latter term is difficult to model because the frictional forces due to O-ring sealing consist of a complex phenomenon as there are many factors in play that have reciprocal influence [18,19]. To simplify the modelling, $F_{O\text{-}rings}(t)$ is obtained through the following phenomenological approach:

$$F_{O-rings}(t) = F_s \cdot H(t_R - t) + \beta \cdot P_R(t) \cdot (1 - H(t_R - t)) \tag{8}$$

where $H(t_R\text{-}t)$ is the Heaviside function and t_R is a time constant. The frictional force takes on this simple expression with the first term modeling the separation friction F_s, which consists of an initial force that is overcome under the initial high load in order to break static friction and generate piston movement. The second term is required for diminishing friction after the piston reaches the sliding value once static friction is overcome.

3. Results and Discussion

The results of the injection process using the combustible mixture at an initial pressure ranging from 25 kPa and 50 kPa are given in Figure 4. Overall, the pressure profiles shown in the figure

reveal a typical needle-free liquid jet evolution with a damped oscillatory behavior. For comparison, a black-colored pressure trace obtained in [18] using an air-powered injector is shown in Figure 5 and similar damped harmonic oscillations can be seen between these two results. However, due to a more severe piston driving condition by the gaseous detonation wave, the damping rate primarily due to friction forces by the O-ring seal and other losses is slower. The more pronounced oscillatory dynamics when compared to the air-powered injection system can also be attributed to the resonant oscillations induced by the multiple wave reflections transmitted from the piston to the water column and impedance mismatch. Nevertheless, a pressure peak is seen upon the detonation wave impacting and driving forward the injector's piston. Subsequently, the jet pressure decays but oscillates. As previous studies describe, it is the initial pressure peak which is important in the formation of a fracture in the skin and the subsequent stabilization to the average delivery pressure determines the depth at which the medication is delivered [43].

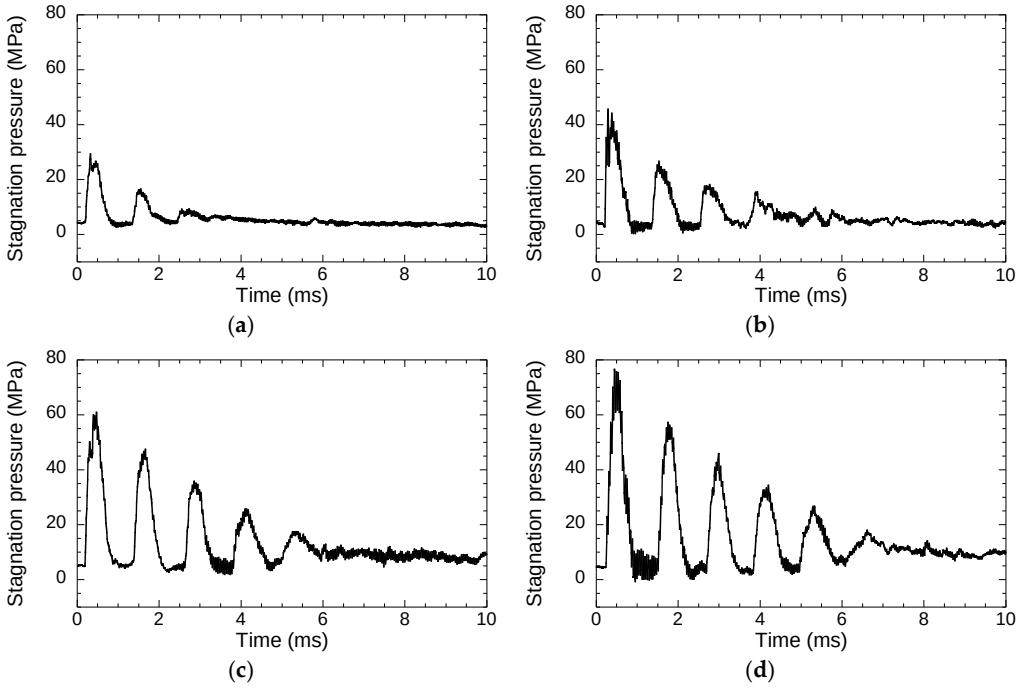

Figure 4. Sample pressure traces from the experiment with combustible initial pressures of (**a**) 25 kPa; (**b**) 30 kPa; (**c**) 40 kPa and (**d**) 50 kPa.

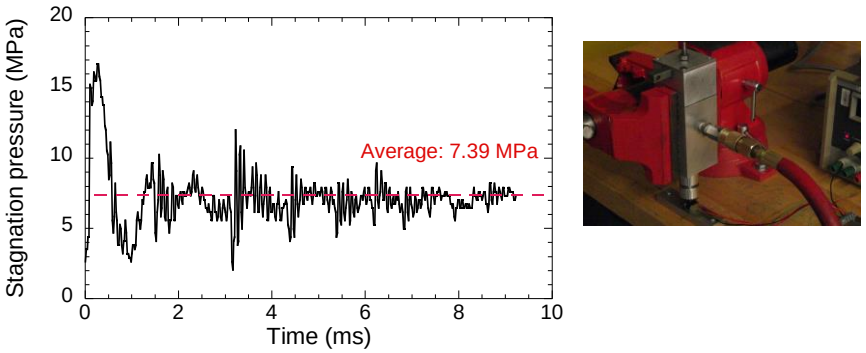

Figure 5. A picture of the in-house air-powered injector and sample pressure trace taken from the air-powered injection experiment [18] with a driving pressure of 413 kPa and orifice nozzle diameter of 200 µm. The pressure was obtained using a different force sensor (Honeywell FSG15N1A). Figure reproduced with the permission of Springer Nature, Journal of Medical and Biological Engineering, Copyright © 2015, Taiwanese Society of Biomedical Engineering.

By increasing the initial pressure of the combustible, hence the pressure across the detonation wave and the reflected detonation-shock, some change in the dynamic behavior of the jet pressure can be observed. Clearly, a longer injection duration can be achieved by increasing the initial pressure also shown by an increasing number of oscillation cycles. At high initial combustible mixture (i.e., above 40 kPa), the injection pressure can be maintained at a sufficient level for a reasonable time duration, at least 5 ms for the present setup. The pressure oscillates with decreasing amplitude around a mean value over a long period of time, which is referred to as the average injection pressure.

By numerically approximating the solutions of Equations (7) and (8) and using experimental data to determine necessary fitting parameters (i.e., τ = 300 µs similar to the value given in [41]; t_R = 0.4 ms; F_s = 1000 to 2800 with increasing initial pressure and $\beta = 2.0 \times 10^{-4}$ for O-ring seals), Figure 6 shows the jet pressure evolution predicted from the analytical model for the combustible initial pressures of 30, 40 and 50 kPa. The experimental results (plotted as dotted curves) are also included for comparison in Figure 6. In general, the model result demonstrates good agreement with the experimental data. The oscillatory evolution, as well as the two main jet properties namely the peak and average stagnation pressures were captured clearly by the model and the values are quantitatively close to the experimental measurements. However, it is important to note that due to the simplicity of the empirical friction model for O-ring seals used in this work, the oscillations cannot be simulated precisely. In order to capture these oscillations (or experimentally eliminate these oscillations), all sources leading to the damping need to be carefully investigated and modeled.

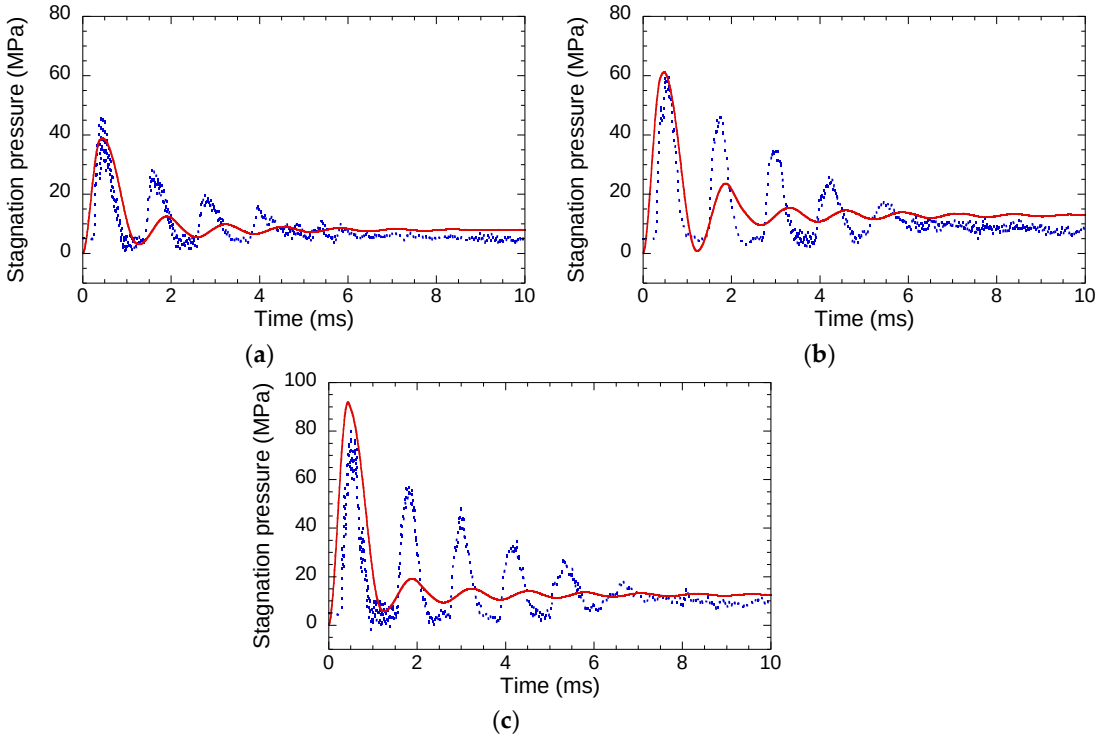

Figure 6. Stagnation pressure evolution from the analytical model with combustible initial pressures of (**a**) 30 kPa; (**b**) 40 kPa and (**c**) 50 kPa.

It is worth noting, that unlike the water hammer effect, which describes pressure variations in a pipeline of which the pressure wave dynamics and damped oscillatory behavior can be accurately obtained using the method of characteristics [44,45], the present liquid jet injection phenomenon also involves a detailed analysis of complete system dynamics, i.e., the fluid-structure interaction between the rapidly moving piston, water column and the flow behind the reflected shock, after the detonation impact. Typically, the water hammer effect is a result of a rapid closing of valves in a flow stream, causing a pressure wave to propagate upstream in the pipe. For such a situation, the numerical solutions

to the water-hammer equations governing the propagation of the pressure surge can predict the wave velocity and damping of the pressure oscillations. It is worth mentioning that an equivalent analysis has been considered by Baker and Sanders [10], referred to as "wave analysis". This study illustrates that the wave analysis results were only valid over a very short time span, i.e., the short duration over which the first pressure spike occurs and when piston movement is negligible and assumed to be zero. Unlike the water-hammer effect, the present phenomenon involves piston acceleration to a high velocity which is no longer negligible, and the water-hammer equations are not sufficient to describe the full dynamics of the injection pressure profile evolution. The continuum analysis approach detailed in Baker and Sanders has become a standard model with continuous improvement for different types of needle-free liquid injection devices driven by a high-velocity plunger, e.g., [15,18,28,32] and thus, is also used in this work. It is important to note that the oscillatory behavior, i.e., both the amplitude and damping of the jet pressure variation are not simply wave dynamics within the liquid column, moreover, they do not solely depend on the liquid acoustic and thermodynamic properties. The oscillatory behavior is a result of system dynamics, which must be modeled considering piston movement caused by the driving force and subsequently countered by the frictional and fluid forces which arise due to the piston movement [10]. All these aforementioned effects are taken into consideration in the continuum analysis, although more accurate quantitative sub-models, e.g., O-ring seals and piston driving force by the detonation wave, are needed to precisely capture the damping of the jet pressure oscillation. Despite the simplicity, the model does capture the two main jet properties, namely, the peak and average stagnation pressure values, and the period of oscillations correlate well to experimental observations. Qualitatively, in our previous work, the effects that strongly influence damping are identified [18]. The friction from sealing is found to be dominant and the oscillations are caused primarily by the piston dynamics. Nevertheless, the liquid viscosity, as can be seen in this study, is also another damping parameter which affects the oscillatory behavior [19,46]. In order to further improve the continuum analysis and obtain more accurate predictions of the jet pressure oscillation, future work will implement an improved quantitative description of the arising frictional force due to the O-ring seals and the detonation reflection process interacting with an accelerating piston.

The pressure traces from both the experimental measurement and analytical results depict both the peak and average jet pressures for different acetylene-oxygen gas mixtures and initial pressures, as can be seen in Figure 7. The solid line represents the analytical model results. For each initial pressure condition, at least five experimental shots were performed. From Figure 7, one can observe immediately that using a detonation-driven controlled release mechanism, the peak stagnation pressure values achieved are much larger than those obtained by air-powered or spring-loaded injector devices which are typically limited in the range below 50 MPa. It is also worth noting that from [47], it is reported that a threshold of 14 MPa is needed for the injection pressure before the jet is able to penetrate into human skin. The present detonation-driven injector easily reaches this threshold and in fact provides initially a much stronger penetration capability compared to the conventional air-powered or spring-loaded devices. The stagnation pressure also makes the computation of jet velocity over the diameter of the orifice possible by using the Bernoulli's equation $V_{jet} = (2P_{jet}/\rho_o)^{1/2}$. The peak jet velocity and average injection velocity correspond to approximately 250–420 m/s and 130–190 m/s range, respectively.

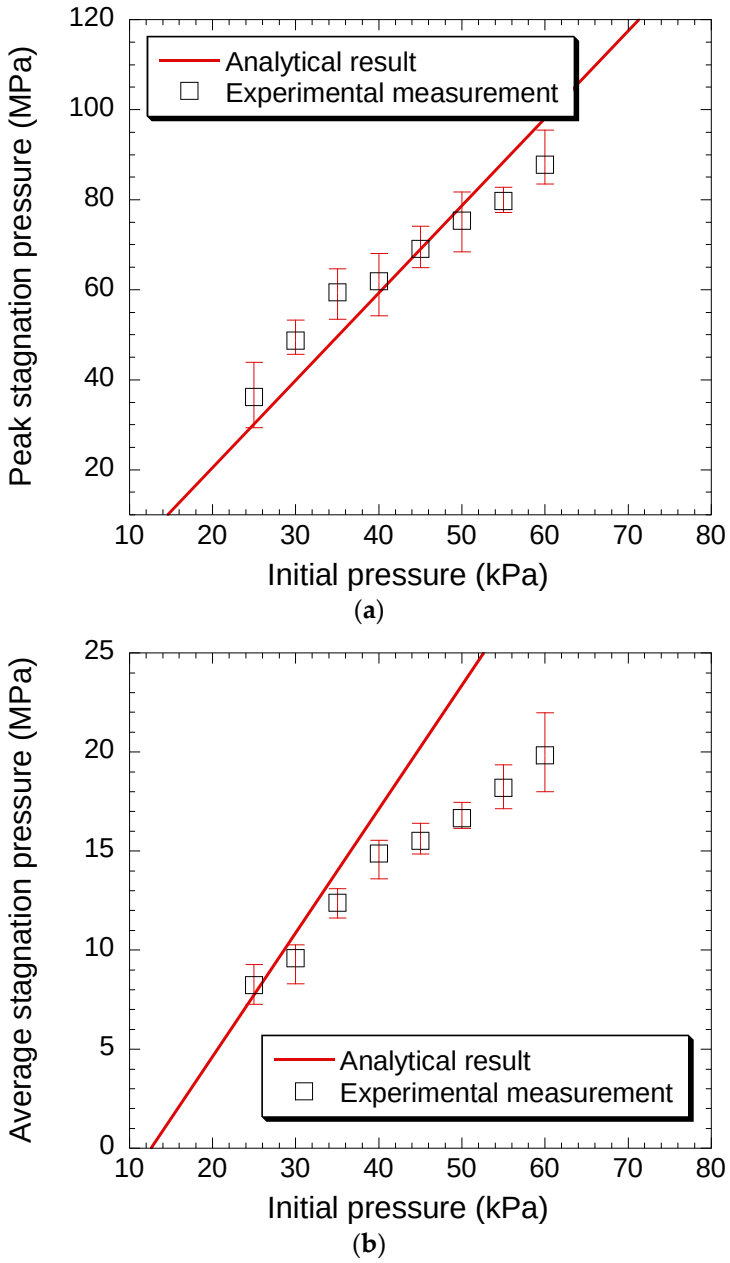

Figure 7. Results of the (**a**) peak pressure; and (**b**) average stagnation pressures as a function of the combustible initial pressure, respectively. The solid lines represent the model results.

As discussed previously, modeling the frictional losses due to the O-ring seal is very challenging. Because of the high-pressure loading condition due to the detonation reflection, experienced by the piston mechanism, it is difficult to establish an exact expression for the level of friction involved and hence, explain the noticeable discrepancy observed in Figure 7 at higher initial pressure. In fact, the average injection pressure is closely related to the piston displacement and hence, a better agreement can perhaps be achieved by modeling the dynamic friction as a function of the piston velocity. This is a future work to improve the accuracy of the present modelling approach.

Furthermore, for the average stagnation pressure driven later by the state behind the Taylor wave expansion, the experimental measurement in general agrees well with the modeled results in the initial pressure range of 25–40 kPa. Note that in the present study, a constant value of the time decay τ is used to obtain the model solutions (see Equation (2)). The reflection time decay may differ and also should be a function of the injector dimension (i.e., length) and initial pressure of the combustible

mixture. Further pressure measurements inside the tube are also needed to accurately determine the time decay constant.

Injections on 60-mm thick ballistics gel with a bloom number of 250 are also performed to visualize the resulting injection and demonstrate the ability of the detonation-driven injector device for deep penetration. Similarly, five experimental shots at each initial pressure are carried out. The results are shown in Figure 8, which seem to depict a linear trend for penetration into the ballistic gel as a function of initial mixture pressure. It is worth noting, that in this study, all the liquid dose in the injection chamber is administrated. The consistent penetration depths from each shot and each condition provide an indication that repetition of injection dosage into the gels is achieved.

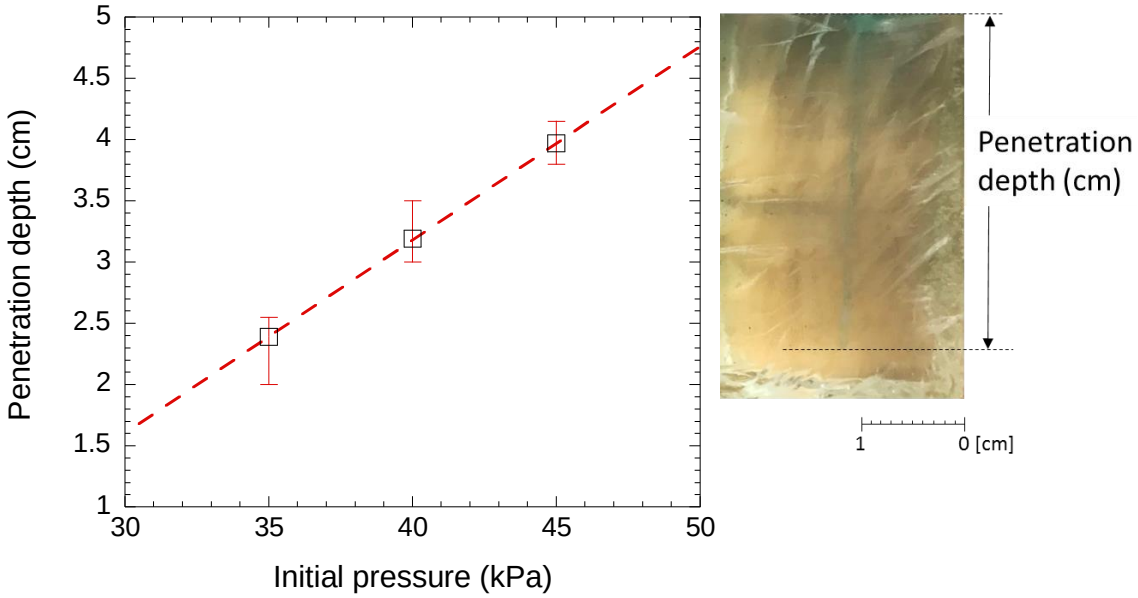

Figure 8. A liquid jet injection by the present detonation-driven injector device into a bloom 250 10% wt. gel as a function of mixture initial pressure.

It is worth noting that the motivation for this study is to design an injector capable of injecting highly viscous liquid. In order to verify the viability of using the present detonation-driven needleless injection concept, tests using mixtures of glycerol/water in the injection are performed. The tested solutions are 30%, 50% and 70% glycerol by weight. Sample jet stagnation pressure evolutions using a combustible initial pressure of 40 and 45 kPa are illustrated in Figure 9. Overall, the injection dynamics do not vary significantly when compared to water (see Figure 4), despite a decrease in the peak stagnation value. Similar dynamic behavior is also observed by further increasing the glycerol content and when using a high initial combustible pressure for detonation, as shown in Figure 10. The main effect of viscosity with the increase of glycerol only decreases the jet stagnation pressure. The variation of peak and average stagnation pressures as a function of % glycerol in the tested liquid solution are plotted in Figure 11. It illustrates that the addition of glycerol content decreases the jet stagnation pressure approximately linearly due to the effect of increasing viscosity [46].

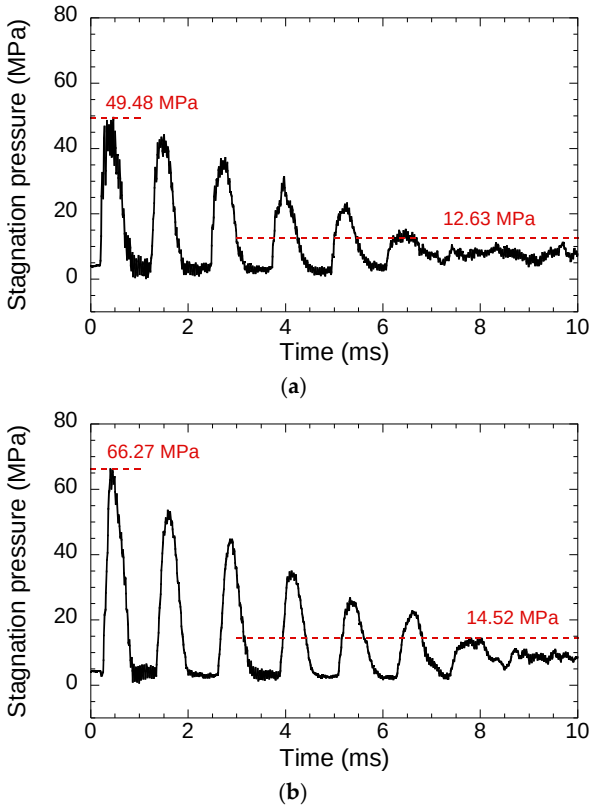

Figure 9. Injection of a solution with 30% (by weight) glycerol using the present detonation-driven injector device with (**a**) 40kPa and (**b**) 45 kPa initial combustible pressure.

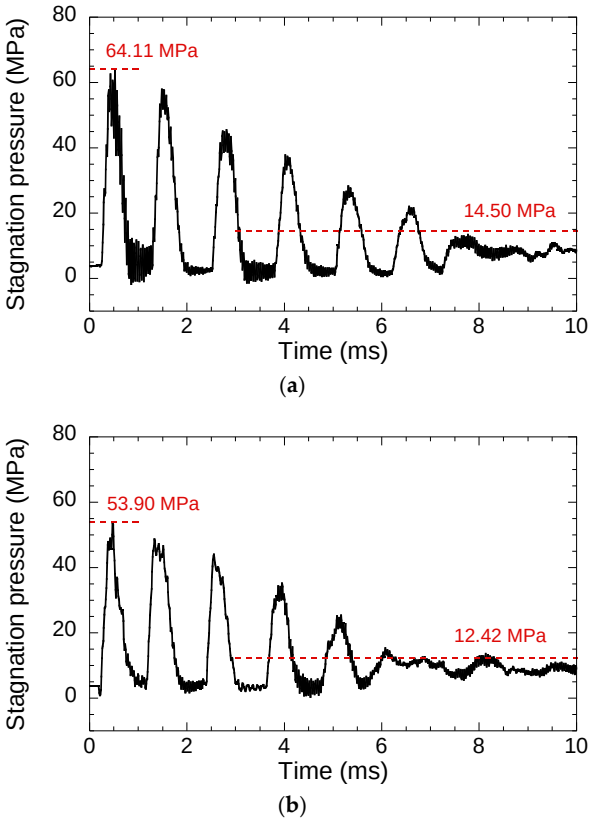

Figure 10. Injection of a solution with (**a**) 50% (by weight) and (**b**) 70% glycerol using the present detonation-driven injector device with an initial combustible pressure of 45 kPa.

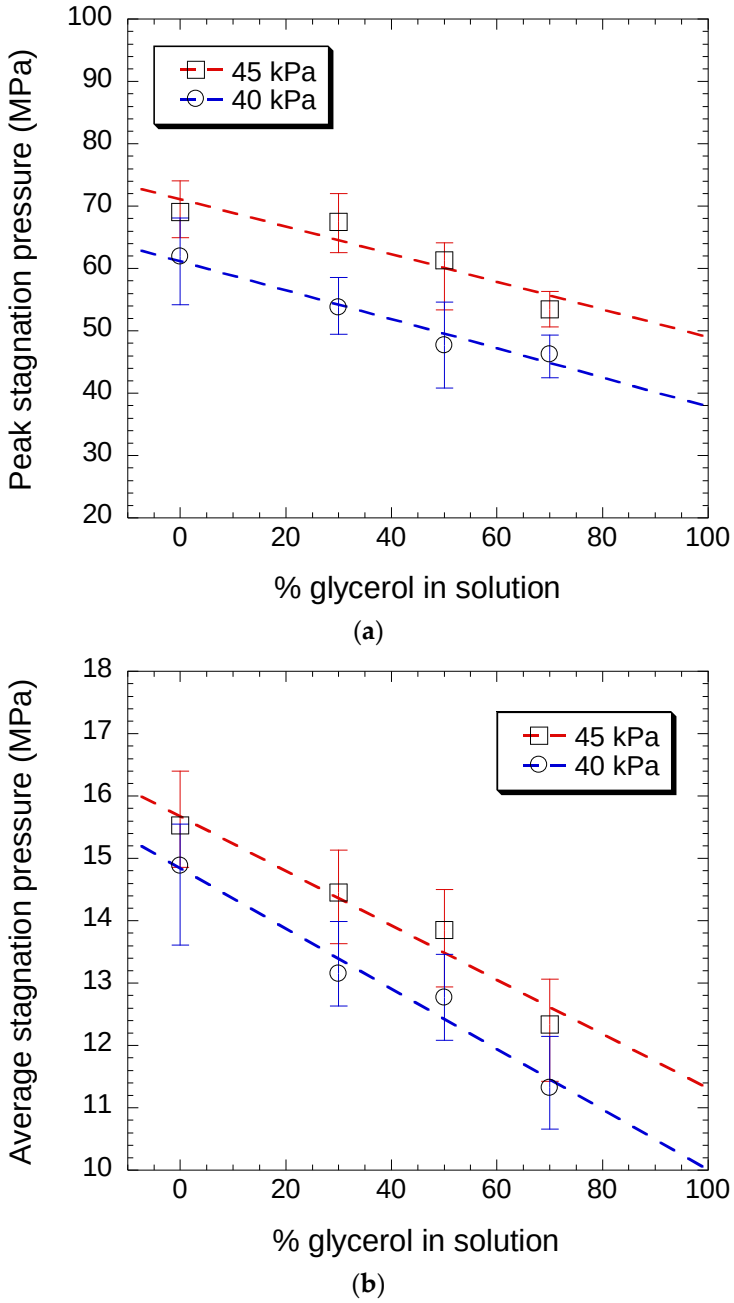

Figure 11. Results of the (**a**) peak pressure; and (**b**) average stagnation pressures as a function of the % glycerol in the solution, respectively. The dashed lines show the trend lines of the experimental results.

4. Conclusions

This study highlights the use of the detonative combustion phenomenon as a novel, alternative energy source to power a conventional mechanical piston-type needle-free liquid jet injector. The comparison with jet pressure measurement of standard air-powered needle-free injectors, illustrates that the detonation-driven device provides equivalent jet injection evolution. However, taking advantage of the pressure rise across a detonation, the combustion-driven device can provide driving forces much larger than those obtained by typical air-powered or spring-loaded injection devices.

Moreover, this study provides promising evidence that a gaseous detonation wave can generate sufficient power to drive a needle-free injector, producing a strong liquid jet applicable for highly viscous drug delivery to meet the requirements of recently emerging medical treatment. On-going work includes the characterization of the jet as a function of the detonation properties, using a number of

combustible mixtures at different initial conditions and its evolution with increasing fluid viscosity [46]. Furthermore, in order to improve both the device performance and modelling output, it is crucial to investigate in more detail the damping caused by various sources and develop a more complete model to describe all the friction losses in the system.

For proof of concept, this study relied on the initiation of the detonation wave via direct initiation by a high-voltage capacitor discharge and the use of a large-scale device. The feasibility of scaling or miniaturizing such a device for practical applications is possible. Recent studies on flame acceleration and the deflagration-to-detonation transition (DDT) in microscale tubes [48–50] provide the opportunity to develop such miniature detonation-driven needle-free injectors. To this end, minimizing the influence of viscous effects and heat losses to the walls becomes the key issue for practical use of this proposed technique.

Author Contributions: Conceptualization, R.P. and H.N.; methodology, R.P. and J.S.; Investigation, R.P., J.S. and H.X.; Formal analysis, R.P. and H.N.; writing—original draft preparation, H.N.; writing—review and editing, R.P. and H.N.

Funding: This work was supported by the Natural Sciences and Engineering Research of Canada NSERC (No. RGPIN-2017-06698).

Conflicts of Interest: The authors declare no conflict of interest.

References

1. Mitragotri, S. Immunization without needles. *Nat. Rev. Immunol.* **2005**, *5*, 905–917. [CrossRef] [PubMed]
2. Baxter, J.; Mitragotri, S. Needle-free liquid jet injections: Mechanisms and applications. *Expert Rev. Med. Devices* **2006**, *3*, 565–574. [CrossRef] [PubMed]
3. Mitragotri, S. Current status and future prospects of needle free liquid jet injectors. *Nat. Rev. Drug Discov.* **2006**, *5*, 543–548. [CrossRef] [PubMed]
4. Hingson, R.A.; Davis, H.S.; Rosen, M. Historical development of jet injection and envisioned uses in mass immunization and mass therapy based upon 2 decades experience. *Mil. Med.* **1963**, *128*, 516–524. [CrossRef]
5. Wijsmuller, G.; Snider, D.E., Jr. Skin testing: A comparison of the jet injector with the Mantoux method. *Am. Rev. Respir. Dis.* **1975**, *112*, 789–798. [PubMed]
6. Schneider, U.; Birnbacher, R.; Schober, E. Painfulness of needle and jet injection in children with diabetes mellitus. *Eur. J. Pediatr.* **1994**, *153*, 409–410. [CrossRef] [PubMed]
7. Raviprakash, K.; Porter, K.R. Needle-free injection of DNA vaccines: A brief overview and methodology. *Methods. Mol. Med.* **2006**, *127*, 83–89. [PubMed]
8. Fargnoli, A.S.; Katz, M.G.; Williams, R.D.; Marguilles, K.B.; Bridges, C.R. A needleless liquid jet injection delivery method for cardiac gene therapy: A comparative evaluation versus standard routes of delivery reveals enhanced therapeutic retention and cardiac specific gene expression. *J. Cardiovasc. Trans. Res.* **2014**, *7*, 756–767. [CrossRef]
9. Kendall, M. Engineering of needle-free physical methods to target epidermal cells for DNA vaccination. *Vaccine* **2006**, *24*, 4651–4656. [CrossRef]
10. Baker, A.B.; Sanders, J.E. Fluid mechanics analysis of a spring-loaded jet injector. *IEEE Trans. Biomed. Eng.* **1999**, *46*, 235–242. [CrossRef]
11. Schramm, J.R.; Mitragotri, S. Transdermal drug delivery by jet injectors: Energetics of jet formation and penetration. *Pharm. Res.* **2002**, *19*, 1673–1679. [CrossRef] [PubMed]
12. Schramm-Baxter, J.; Mitragotri, S. Needle-free jet injections: Dependence of jet penetration and dispersion in the skin on jet power. *J. Control. Release* **2004**, *97*, 527–535. [CrossRef] [PubMed]
13. Brown, M.B.; Martin, G.P.; Jones, S.A.; Akomeah, F.K. Dermal and transdermal drug delivery systems: Current and future prospects. *Drug Deliv.* **2006**, *13*, 175–187. [CrossRef] [PubMed]
14. Chen, K.; Zhou, H.; Li, J.; Cheng, G.J. A model on liquid penetration into soft material with application to needle-free jet injection. *Asme J. Biomech. Eng.* **2010**, *132*, 101005. [CrossRef] [PubMed]
15. Chen, K.; Zhou, H.; Li, J.; Cheng, G. Stagnation pressure in liquid needle-free injection: Modeling and experimental validation. *J. Drug Deliv. Lett.* **2011**, *1*, 97–104.

16. Baxter, J.; Mitragotri, S. Jet-induced skin puncture and its impact on needle-free jet injections: Experimental studies and a predictive model. *J. Control. Release* **2005**, *106*, 361–373. [CrossRef] [PubMed]
17. Mohanty, C.; Mannavathy, C.; Srikanth, D.; Tabassum, R. Needle free drug delivery systems: A review. *Int. J. Pharm. Res. Dev. Ijprd* **2011**, *3*, 7–15.
18. Portaro, R.; Ng, H.D. Experiments and modeling of air-powered needle free liquid injectors. *J. Med. Biol. Eng.* **2015**, *35*, 685–695. [CrossRef]
19. Nakayama, H.; Portaro, R.; Kiyanda, C.B.; Ng, H.D. CFD modeling and validation of high speed liquid jets from an air-powered needle-free injection system. *J. Mech. Med. Biol.* **2015**, *16*, 1650045. [CrossRef]
20. Taberner, A.; Hogan, N.C.; Hunter, I.W. Needle-free jet injection using real-time controlled linear Lorentz-force actuators. *Med. Eng. Phys.* **2012**, *34*, 1228–1235. [CrossRef]
21. Li, X.; Ruddy, B.; Taberner, A. Characterization of needle-assisted jet injections. *J. Control. Release* **2016**, *243*, 195–203. [CrossRef] [PubMed]
22. Ruddy, B.; Dixon, A.; Williams, R.; Taberner, A. Optimization of portable electronically-controlled needle-free jet injection systems. *IEEE/Asme Trans. Mechatron.* **2017**, *22*, 2013–2021. [CrossRef]
23. Fletcher, D.A.; Palanker, D.V. Pulsed liquid microjet for microsurgery. *Appl. Phys. Lett.* **2001**, *78*, 1933–1935. [CrossRef]
24. Tagawa, Y.; Oudalov, N.; Visser, C.W.; Peters, I.R.; van der Meer, D.; Sun, C.; Prosperetti, A.; Lohse, D. Highly focused supersonic microjets. *Phys. Rev. X* **2012**, *2*, 031002. [CrossRef]
25. Menezes, V.; Nakagawa, A.; Takayama, K. Laser-based pulsed liquid microjet for surgery. *J. Indian Inst. Sci.* **2006**, *86*, 207–214.
26. Berrospe-Rodriguez, C.; Visser, C.W.; Schlautmann, S.; Ramos-Garcia, R.; Fernandez Rivas, D. Continuous-wave laser generated jets for needle free applications. *Biomicrofluidics* **2016**, *10*, 014104. [CrossRef] [PubMed]
27. McKeage, J.W.; Ruddy, B.P.; Nielsen, P.M.F.; Taberner, A.J. The effect of jet speed on large volume jet injection. *J. Control. Release* **2018**, *280*, 51–57. [CrossRef] [PubMed]
28. Williams, R.M.J.; Ruddy, B.P.; Hogan, N.C.; Hunter, I.W.; Nielsen, P.M.F.; Taberner, A.J. Analysis of moving-coil actuator jet injectors for viscous fluids. *IEEE Trans. Biomed. Eng.* **2016**, *63*, 1099–1106. [CrossRef]
29. Rao, S.S.; Gomez, P.; Mascola, J.R.; Dang, V.; Krivulka, G.R.; Yu, F.; Lord, C.I.; Shen, L.; Bailer, R.; Nabel, G.J.; et al. Comparative evaluation of three different intramuscular delivery methods for DNA immunization in a nonhuman primate animal model. *Vaccine* **2006**, *24*, 367–373. [CrossRef]
30. Chase, C.C.; Daniels, C.S.; Garcia, R. Needle-free injection technology in swine: Progress toward vaccine efficacy and pork quality. *J. Swine Health Prod.* **2008**, *16*, 254–261.
31. Mousel, M.R.; Leeds, T.D.; White, S.N.; Herrmann-Hoesing, L.M. Technical note: Comparison of traditional needle vaccination with pneumatic, needle-free vaccination for sheep. *J. Anim. Sci.* **2008**, *86*, 1468–1471. [CrossRef] [PubMed]
32. Chen, K.; Pan, M.; Liu, T. Design and analysis of a continuous split typed needle-free injection system for animal vaccination. *Open Biomed. Eng. J.* **2017**, *11*, 59–71. [CrossRef] [PubMed]
33. Wolanski, P. Detonative propulsion. *Proc. Combust. Inst.* **2013**, *34*, 125–158. [CrossRef]
34. Vasil'ev, V.V. The principle aspects of application of detonation in propulsion systems. *J. Combust.* **2013**, 945161.
35. Golub, V.V.; Bazhenova, T.V.; Baklanov, D.I.; Ivanov, K.V.; Kirvokorytov, M.S. Using of hydrogen-air mixture detonation in needle-free injection devices. *High Temp.* **2013**, *51*, 138–140. [CrossRef]
36. Krivokoritov, M.; Baklanov, D.; Golub, V.; Ivanov, K. Application of Gas Detonation for a Needleless Device Development. In Proceedings of the 28th International Symposium on Shock Waves, Manchester, UK, 17–22 July 2012; Kontis, K., Ed.; Springer: Berlin/Heidelberg, Germany, 2012; pp. 403–407.
37. Gordon, S.; McBride, B.J. *Computer Program for Calculation of Complex Chemical Equilibrium Compositions and Applications, Technical Report 1311*; NASA Reference Publication; NASA: Washington, DC, USA, 1994.
38. Stanyukovich, K.P. *Unsteady Motion of Continuous Media*; Pergamon Press: New York, NY, USA, 1960.
39. Shepherd, J.E.; Teodorczyk, A.; Knystautas, R.; Lee, J.H.S. Shock waves produced by reflected detonations. *Prog. Astro. Aero.* **1991**, *134*, 244–264.
40. Beltman, W.M.; Shepherd, J.E. Linear elastic response of tubes to internal detonation loading. *J. Sound Vib.* **2002**, *252*, 617–655. [CrossRef]
41. Karnesky, J.; Damazo, J.; Chow-Yee, K.; Rusinek, A.; Shepherd, J. Plastic deformation due to reflected detonation. *Int. J. Solids Struct.* **2013**, *50*, 97–110. [CrossRef]

42. Damazo, J.; Shepherd, J.E. Observations on the normal reflection of gaseous detonations. *Shock Waves* **2017**, *27*, 795–810. [CrossRef]
43. Arora, A.; Hakim, I.; Baxter, J.; Rathnasingham, R.; Srinivasan, R.; Mitragotri, S. Needle free delivery of macromolecules across the skin by nanolitre-volume pulsed microjets. *Proc. Nat. Acad. Sci. USA* **2007**, *104*, 4255–4260. [CrossRef]
44. Ghidaoui, M.S.; Zhao, M.; McInnis, D.A.; Axworthy, D.H. A review of water hammer theory and practice. *Appl. Mech. Rev.* **2005**, *58*, 49–76. [CrossRef]
45. Kumar, A.; Prasad, P.S.; Rao, M.R. Experimental studies of water hammer in propellant feed system of reaction control system. *Propul. Power Res.* **2018**, *7*, 52–59. [CrossRef]
46. Portaro, R.; Nakayama, H.; Ng, H.D. Optimization of drug viscosity used in gas-powered liquid jet injectors. In Proceedings of the Annual International Conference of the IEEE Engineering in Medicine and Biology Society (EMBC), Milan, Italy, 25–29 August 2015.
47. Shergold, O.A.; Fleck, N.A. Mechanisms of deep penetration of soft solids, with application to the injection and wounding of skin. *Proc. Roy. Soc. Lond. A* **2004**, *460*, 3037–3058. [CrossRef]
48. Wu, M.H.; Burke, M.P.; Son, S.F.; Yetter, R.A. Flame acceleration and the transition to detonation of stoichiometric ethylene/oxygen in microscale tubes. *Proc. Combust. Inst.* **2007**, *31*, 2429–2436. [CrossRef]
49. Wu, M.H.; Wang, C.Y. Reaction propagation modes in millimeter-scale tubes for ethylene/oxygen mixtures. *Proc. Combust. Inst.* **2011**, *33*, 2287–2293. [CrossRef]
50. Han, W.; Yang, G.; Law, C.K. Flame acceleration and deflagration-to-detonation transition in micro- and macrochannels: An integrated mechanistic study. *Combust. Flame* **2017**, *176*, 285–298. [CrossRef]